Excitonic effects in coupled quantum wells

A. M. Fox,* D. A. B. Miller, G. Livescu,† J. E. Cunningham, and W. Y. Jan
AT&T Bell Laboratories, Crawfords Corner Road, Holmdel, New Jersey 07733
(Received 29 November 1990; revised manuscript received 2 May 1991)

Electron-sublevel-anticrossing effects have been studied in coupled quantum wells where the exciton binding energy is comparable to the minimum sublevel splitting. The anticrossing was induced by applying an electric field to align the first and second sublevels of adjacent wells. In this situation the electron-hole Coulomb interaction has a strong effect on the splittings measured by optical techniques, because the optical spectra typically measure exciton energies rather than single-particle energies. The most striking effect is that the minimum splitting of the excitons associated with each of the split electron levels does not occur at the same field as for the minimum splitting of the bare-electron levels. One unexpected but readily observable consequence is that when the same electron-sublevel splitting is measured using two different pairs of intrawell and interwell exciton transitions, the field for minimum exciton splitting can differ by up to $\sim 10\%$ from one pair of transitions to the other. We have constructed a variational model of the coupled excitons that explains these effects in terms of Coulomb mixing of the delocalized electron states. We have measured the exciton splittings directly by photocurrent spectroscopy in three $GaAs/Al_{0.3}Ga_{0.7}As$ multiple-quantum-well structures. The samples were similar in design except that the $Al_xGa_{1-x}As$ barrier thickness varied from 15 to 35 Å. By fitting our variational model to the experimental anticrossing data, we have been able to deduce the actual bare-electron level splittings rather than the exciton splittings. Within the experimental accuracy, we find that the minimum splitting decreased exponentially with increasing barrier thickness, as would be expected for simple quantum-mechanical tunneling.

I. INTRODUCTION

The anticrossing of energy levels brought into degeneracy is a well-known property of quantum-mechanical systems. This anticrossing physics extends directly across to the growing research field of coupled semiconductor quantum wells. These structures consist of two or more quantum wells separated from each other by thin barriers. The simplest case is that of two identical wells, which was considered theoretically by Kane in 1967.[1] He derived an analytic formalism for calculating the splitting ΔE of the otherwise degenerate sublevels of the individual wells caused by the coupling through the barrier. The work of Kazarinov and Suris in 1971 opened up another dimension to the problem, when they considered the case of resonant coupling induced by an external electric field.[2] When the electric field F is applied perpendicular to the plane of the quantum wells, it adjusts the potential of one well with respect to its nearest neighbors, as shown for the case of two identical wells in Fig. 1(a). For most applied fields, the structure behaves like two isolated wells, with the particles localized predominantly in just one of the wells. However, at certain key resonant fields F_{res}, the levels of the adjacent wells line up with each other. At these resonant fields, the levels become delocalized and extend across both wells [see Fig. 1(b)]. Because of the finite coupling through the barrier, the levels repel each other as they are brought into resonance, showing anticrossing behavior with a minimum level separation ΔE.

Experimental and theoretical interest in coupled quantum wells has advanced considerably over the last five years or so, paralleling the advances in epitaxial growth of quantum structures. This research is prompted both by basic interest in the coupling physics and also by potential application of coupled quantum wells in optoelectronic devices. There has been a great deal of work on measuring and understanding the electronic and optical properties of these systems, in a variety of material systems.[3–34] Much of the work focuses on understanding and measuring the coupled states at the resonant field, either for coupled electrons[3–26] or holes.[22,27,28] There have also been a number of experimental and theoretical studies which concentrate specifically on the nature of the excitons in coupled quantum wells,[22,29–33] including the recent exciting observation of an excitonic phase transition in such systems.[34] From the point of view of both basic physics and also device optimization, it is essential to be able to determine ΔE accurately. To date, all attempts to measure ΔE have used optical spectroscopy, in which the exciton energies are followed as the applied field is swept through the resonance.[3,10,12,15,29,33] Close to the resonant field the anticrossing of the levels is reflected in the absorption or photoluminescence spectra as a splitting between the two exciton lines associated with each of the two split levels. In the simplest picture of the coupling, the exciton energies simply follow those of the resonant single-particle levels, and ΔE can be extracted directly from the spectra as the minimum splitting of the exciton lines. However, it is obvious from this single-particle picture is too simplistic, because the exciton binding energy (5–10 meV) is of the same magnitude as ΔE for many

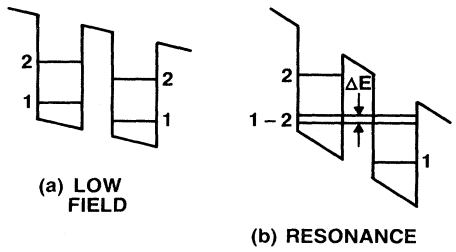

FIG. 1. Two coupled quantum wells in an applied perpendicular electric field, each with two confined states per well: (a) below resonance, (b) at resonance. ΔE is the level splitting at the resonant field.

coupled wells. It is therefore to be expected that Coulomb effects will cause significant alterations to the measured spectra.

In this work we study coupled-quantum-well effects in multiple-quantum-well structures, rather than the coupled-double-well structure sketched in Fig. 1. At low fields these multiple-quantum-well samples behave like superlattices, showing miniband formation and Stark-ladder effects.[35] We will consider these low-field effects in a future publication. Here we consider the behavior at high fields, where the superlattice minibands have broken up, and the levels are localized in the individual wells. In this high-field limit, we observe $e1$-$e2$ resonances when the field aligns the first electron sublevel of one well with the second sublevel of its nearest neighbor. The physics of this resonance is essentially the same as for the double-well resonance sketched in Fig. 1(b), only that the resonance is repeated many times throughout the structure for each pair of adjacent wells. Although we have only studied one particular electron resonance, the excitonic effects discussed here are general to all coupled-well systems, including the $e1$-$e1$ resonances in symmetric or asymmetric coupled double quantum wells. The $e1$-$e2$ resonance is particularly interesting to study because there are two distinct ways to observe it: (1) through the (hh1$\rightarrow e1$)-like optical transition; (2) through the (hh1$\rightarrow e2$)-like transition. It is the difference between these two transitions that reveals the effects of the excitons on the coupling.

In our earlier Brief Report,[33] we outlined how the field for minimum exciton line splitting differs from the true resonant field, and the shift varies between the two different types of optical transitions. In the original $GaAs/Al_{0.3}Ga_{0.7}As$ sample, the shift was $\pm 5\%$. Unlike space-charge effects,[11] this is an intrinsic property of the optical transition. The shift cannot be adequately explained in the single-particle picture, and a more complete model is required that includes a full calculation of the field-dependent exciton energies around the resonant field. In this paper, we present data on two new samples with thinner barriers and correspondingly larger values of ΔE. We give a full description of the variational model we have developed to calculate the exciton energies, and compare it to the experimental data on the three samples. In this way we have been able to study the dependence of ΔE on the barrier width both experimentally and theoretically, and to examine how the value for the band-offset ratio for the $GaAs/Al_xGa_{1-x}As$ system affects the results.

The paper is laid out as follows. In Sec. II we describe the design of our three $GaAs/Al_xGa_{1-x}As$ multiple-quantum-well samples. In Sec. III we discuss how the optical properties of a multiple-quantum-well structure are modified close to the resonant field. In Sec. IV we present experimental measurements of the photocurrent spectra of the three samples around the resonance field. In Sec. V we give a qualitative discussion of the results, and in Sec. VI we describe the variational exciton energy calculation which we used to make a quantitative comparison between theory and experiment. In Sec. VII we draw our conclusions.

II. SAMPLE DESIGN

We studied resonant coupling effects in three $GaAs/Al_xGa_{1-x}As$ multiple-quantum-well (MQW) samples. The samples were designed to have a GaAs well thickness L_w of 95 Å with an x value of 0.3 for the barriers, and with the barrier thickness L_b varying from 35 to 15 Å. Table I gives details of the samples as deduced from x-ray measurements. The accuracy of the x-ray measurements is estimated to be $\pm 2\%$, except for the very thin barriers, where the accuracy is closer to 10%. These x-ray measurements tell us that our growth calculation is accurate to about 10%. The number of periods was chosen in order to keep the total nominal MQW thickness to approximately 1.0 μm throughout. The quantum wells were grown as the intrinsic region of a p-i-n structure, so that an approximately uniform electric field could be placed across the quantum wells by applying reverse bias to the diode. 200-μm mesas were etched into the wafers, and the optical window was typically 200×100 μm^2 after making the wire bonds. Resonant coupling effects were also observed in a fourth sample

TABLE I. Sample parameters from growth calibration and x-ray measurements.

Sample	Well width (Å)	Barrier width (Å)	x	Number of periods	Total MQW thickness (μm)
I	86	34	0.34	80	0.96
II	95	23	0.28	93	1.10
III	87	18	0.30	91	0.96

with lower, thicker barriers ($x=0.2$, $L_b=65$ Å). In this sample, the splitting was too small to be resolved even at low temperatures, although the resonant coupling was still detectable by an anomalous exciton line broadening at the resonant field.

Intuitively, we expect that the quantum-mechanical coupling between adjacent wells will be related to the single-particle tunneling probability through the central barrier. This can be calculated from elementary quantum theory to be $\exp\{-2L_b[2m^*(V_0-E)]^{1/2}/\hbar\}$, where L_b is the thickness of the barrier, m^* is the effective mass of the particle in the barrier, V_0 is the barrier height, and E is the particle energy. (A more rigorous justification of this statement based on Kane's formalism is given in Ref. 14.) In this picture we expect the resonant coupling to increase by about an order of magnitude from sample I to sample III.

III. OPTICAL TRANSITIONS

Let us first understand the coupling of the electron levels in adjacent wells, neglecting for the moment the electron-hole Coulomb interaction. In Fig. 2 we sketch a portion of the conduction and valence bands of a MQW in which there are two electron sublevels per well. Three field values close to the $e1$-$e2$ resonant field are considered: (a) F slightly less than $F_{\rm res}$, (b) $F=F_{\rm res}$, and (c) slightly greater than $F_{\rm res}$. For clarity, only the electron and first heavy-hole sublevels of each quantum well are shown. The vertical arrows represent the $n=1$ heavy-hole (hh) optical transitions. Because the field is close to resonance, it is necessary to consider the spreading of the $e1$ and $e2$ levels into their nearest neighbors. This gives rise to spatially "indirect" (interwell) transitions as well as the spatially "direct" (intrawell) transitions.[7] The oscillator strength of these transitions is proportional to the overlap between the localized hh1 level and delocalized electron levels.

Figure 2(b) considers the case of $|F-F_{\rm res}|=0$. At this field strength, the $e1$ and $e2$ levels of adjacent wells would be degenerate in the absence of coupling. The coupling lifts the degeneracy, and gives rise to two states spanning both wells with the minimum separation ΔE between the two levels. The electron probability amplitude is roughly 50% per state per well. This results in *two* strong intrawell optical transitions per well associated with the $n=1$ heavy-hole transition. The energy separation of these two intrawell transitions is ΔE, and each has a relative oscillator strength of ~ 0.5. These two transitions are indicated by the solid vertical arrows in each well in Fig. 2(b).

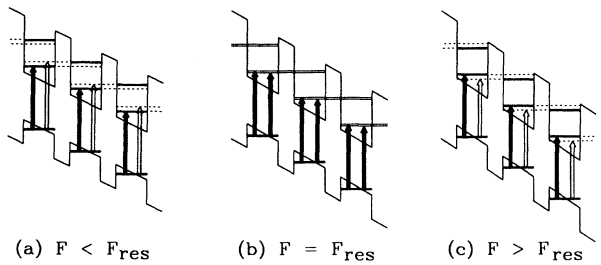

FIG. 2. Schematic band diagram of three wells from within a coupled multiple-quantum-well structure with two electron sublevels per well. For clarity, only the first heavy hole and the electron sublevels are shown. Three field strengths are considered: (a) F slightly less than $F_{\rm res}$, (b) $F=F_{\rm res}$, (c) F slightly greater than $F_{\rm res}$. Solid lines for the levels indicate a large probability amplitude, whereas dashed lines indicate a smaller amplitude. The $n=1$ heavy-hole intrawell transitions are indicated by solid vertical arrows, while interwell transitions are indicated by open arrows.

As $|F-F_{\rm res}|$ increase from 0, the energy separation of the $e1$ and $e2$ levels of adjacent wells increases. The levels become more localized in their own wells, with a corresponding decrease in the probability amplitude in the adjacent well. This is indicated by the solid and dashed lines representing the electron levels in Figs. 2(a) and 2(c), which consider the case where $|F-F_{\rm res}|$ is small but finite. For each well there is now one intrawell transition as indicated by the solid vertical arrows, and a second interwell transition as indicated by the open arrows. The intrawell transition is the stronger of the two because the electron and hole are localized predominantly in the same well, whereas for the interwell transition the electron and hole are predominantly in different wells. In Fig. 2(a) where $F<F_{\rm res}$, the interwell transition has the larger energy, whereas for Fig. 2(c) where $F>F_{\rm res}$, the interwell transition is at the lower energy.

When $|F-F_{\rm res}|$ becomes larger still, the oscillator strength of the interwell transition drops off to the point where it becomes undetectable. In this case it is only necessary to consider the intrawell transitions; the spectra behave like those of a "normal" (uncoupled) multiple-quantum-well structure.

In Fig. 3 we show a three-dimensional (3D) plot of the wave-function amplitude for two resonant $e1$-$e2$ levels of Fig. 2 as the field is swept through resonance. These wave functions were calculated for sample I. At low field we have two well-resolved states with either $e1$ or $e2$ character, with the $e1$-like level at the lower energy. As the field is increased, the two levels begin to mix with each other through the barrier, and at the resonant field (83 kV cm^{-1}), the wave functions have approximately equal $e1$ and $e2$ character. Above $F_{\rm res}$, the levels separate out again and recover their individual $e1$ and $e2$ character. Note that the lower-energy state evolves continuously from an $e1$ state to an $e2$ state, and vice versa, which is obvious from inspection of Fig. 2. However, the levels (and therefore the optical transitions) are uniquely identified at all fields by the number of wave-function nodes in the wells of interest. In the language of molecular physics, the wave function with one node at lower energy is the "bonding" state, while the double-noded higher-energy level is an "antibonding" state.

From the simple description given above, one would expect to be able to determine the minimum level splitting ΔE from studying the energy dependence of the interwell and intrawell optical transitions. However, in order to do this, the photon has to create a hole at the same time as an electron, and the Coulomb interaction can per-

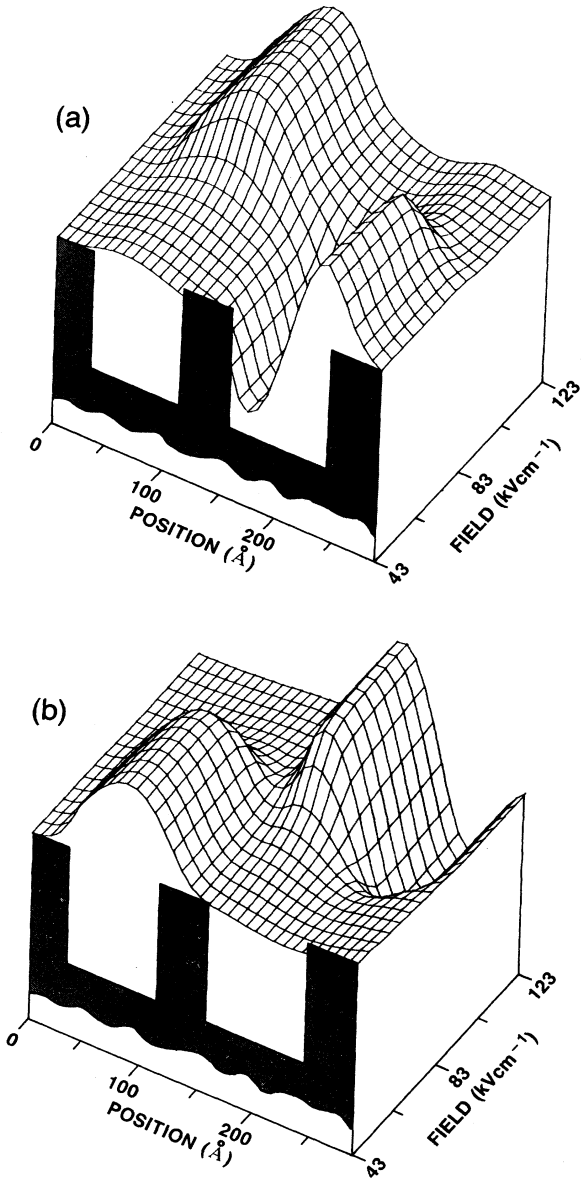

FIG. 3. Coupled "bare" electron wave functions as a function of electric field calculated for sample I. The $e1$-$e2$ resonance occurs at 83 kV cm^{-1} in this structure. Wave function (a) is the double-noded higher-energy "antibonding" level, while wave function (b) is for the single-noded "bonding" level.

turb the wave functions, thereby complicating the analysis. In the sections which follow, we discuss the effect of the electron-hole Coulomb interaction on the measured transition energies.

IV. EXPERIMENTAL RESULTS

Photocurrent spectra were taken for the three samples both at room temperature and at low temperature (≤ 50 K) using a tungsten lamp as the excitation source. With a 0.25-m monochromator, the energy resolution was typically ~ 2 meV. At 300 K we observed a small anomalous broadening in both the $n=1$ heavy- and light-hole exciton absorption lines at 7 V in sample I, while in samples II and III the splitting of the levels at resonance was just resolvable around 8 V. On cooling, the exciton linewidths were very considerably reduced, making for better resolution of the resonant coupling effects. From now on, we shall concentrate exclusively on the low-temperature data.

As an example of the low-temperature spectra, we show in Fig. 4 the photocurrent spectra of sample I at 0, 5.0, and 7.0 V taken at 30 K. We have identified the various transitions that are resolved in the spectra by calculating the energy levels with a tunneling resonance program.[36,37] In our notation, Hij (Lij) refers to a transition from the ith heavy- (light-) hole sublevel to the jth electron sublevel. The "forbidden" transitions with $i \neq j$ become stronger as the voltage increases. Note that at 7.0 V, the $H11$, $L11$, $H21$, and $H31$ transitions are all anomalously broadened. These transitions have in common the fact that they terminate on the $e1$ level, and give an indication of the resonance of the $e1$ and $e2$ sublevels of adjacent wells. This anomalous broadening occurs at the same voltage as measured for the anomalous broadening of the $H11$ transition at room temperature.

In Figs. 5(a)–5(c) we show 3D plots of the band-edge photocurrent spectra of the three samples around the $e1$-$e2$ resonance field. In Figs. 6(a)–6(c) we show the field dependence of the $H11$ exciton lines as a function of applied voltage, as deduced from the spectra, together with a theoretical fit to be discussed below. We will concen-

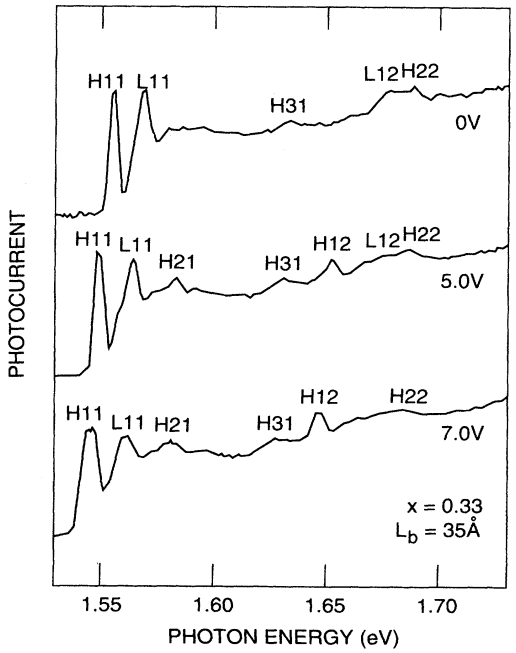

FIG. 4. Photocurrent spectra of sample I at 30 K for 0, 5.0, and 7.0 V reverse bias. The assignment of the resolved transitions was done by comparing the spectrum with the calculated energy levels.

trate first on sample I [Figs. 5(a) and 6(a)]. The $H11$ heavy- and $L11$ light-hole exciton absorption lines dominate the spectra. From the point of view of resonant coupling, the interesting spectral feature can just be discerned in the gap between the heavy- and light-hole exciton lines, at voltages from 6.4 to 7.0 V. We identify this as the $H11_2$ interwell transition. The subscript refers to the number of nodes in the electron wave function. This interwell transition is seen to merge into the high-energy wings of the $H11_1$ line as the voltage is increased. Because the barrier is relatively thick ($L_b = 35$ Å), the resonant-coupling effects are not particularly strong, and the energies of the direct and indirect excitons have to be deconvolved from the spectra. Figure 6(a) shows the energies of the $H11_1$ and $H11_2$ excitons as a function of applied voltage. We observe clear anticrossing behavior for the two levels, with a minimum splitting of ~ 4.5 meV at 7.0 V. Note how the two transitions change character on passing through the resonance field.

Figure 5(b) shows the spectra for sample II near the $e1$-$e2$ resonance field. Since the barrier is thinner than for sample I (25 Å as opposed to 35 Å), we expect to see stronger resonant-coupling effects. This is indeed the case. At 7.0 V the $H11_1$ line is clearly seen in the spectra at 1.537 eV. The oscillator strength of this transition gradually diminishes with increasing voltage. By contrast, the $H11_2$ line, which occurs at a slightly higher energy, is observed to increase in oscillator strength as the voltage is increased. The energy separation of the lines is minimum around 8.4 V, at which point the two lines are clearly resolved in the spectrum, with approximately the same oscillator strength. The voltage dependence of the $H11_1$ and $H11_2$ lines is given in Fig. 6(b). We find a minimum separation of 8.7 meV, which is almost twice as

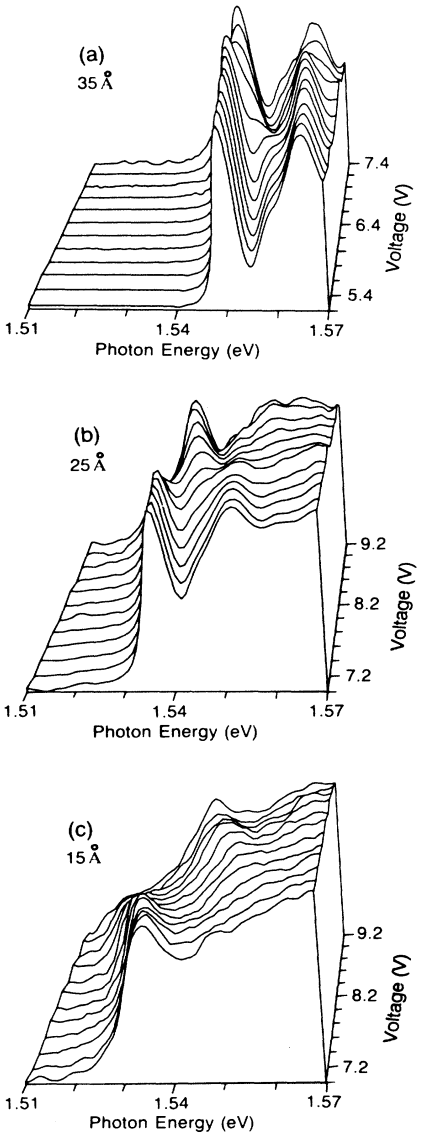

FIG. 5. 3D plots of the band-edge photocurrent spectra as a function of reverse bias. (a) Sample I ($L_b = 35$ Å) at 30 K. (b) Sample II ($L_b = 25$ Å) at 30 K. (c) Sample III ($L_b = 15$ Å) at 50 K.

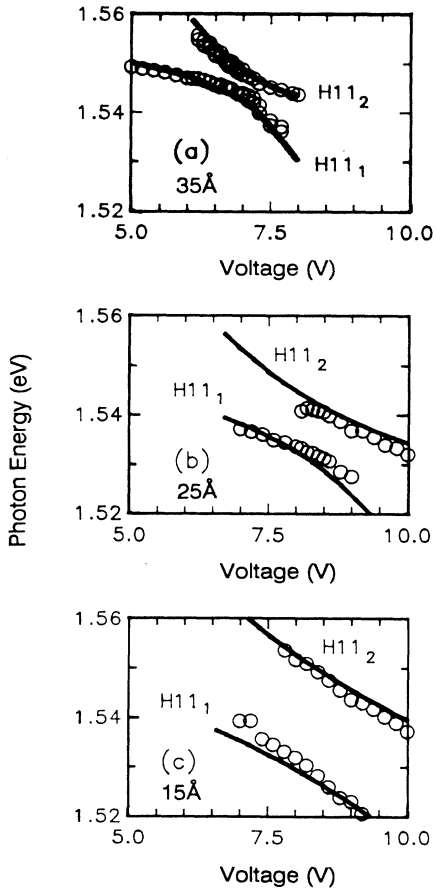

FIG. 6. $H11$ exciton energies versus reverse bias: (a) Sample I, (b) sample II, (c) sample III. The solid lines show the results of a variational calculation of the exciton transition energies described in Sec. VI using the sample parameters given in Table II.

large as for sample I.

Figure 5(c) shows the spectra for sample III. The first point to notice for this sample is that the exciton lines are quite significantly broader than for samples I and II, presumably because of the lifetime broadening by faster tunneling. By the same token, the resonant coupling effects are even stronger than for sample II. The voltage dependence of the $H11_1$ and $H11_2$ excitons is given in Fig. 6(c), from which we see that the minimum splitting is 20.8 meV.

Looking at the data for the three samples presented together in Figs. 5(a)–5(c) and 6(a)–6(c), one of the most striking features is the decrease in ΔE with increasing barrier thickness. As discussed briefly above, this is related to the exponential dependence of the interwell coupling on the barrier thickness. We will return to discuss the dependence of ΔE on the barrier thickness in more detail in Sec. VI.

Referring back to Fig. 2, it is evident that there is an equivalence between the $e1$ and $e2$ levels at the resonant field. Therefore, we would expect to observe a similar anticrossing behavior in optical transitions which terminate on the $e2$ state as well as those terminating on the $e1$ state. The best resolved absorption line around the resonant voltage which terminates on the $e2$ state is the $H12$ forbidden transition in our samples (see Fig. 4). In Figs. 7(a) and 7(b) we show a 3D plot of the spectrum around the $H12$ transition for samples I and II. (We could not resolve the $H12$ transition for sample III.) Figures 8(a) and 8(b) show the corresponding $H12$ exciton energies as a function of applied voltage for the two samples. The anticrossing behavior is evident for both samples. In particular, the anticrossing behavior is much clearer for sample I in the $H12$ transition than for the $H11$ transition. On comparing Figs. 6(a) and 6(b) and 8(a) and 8(b) we notice immediately that in both samples the field dependence of the $H11$ and $H12$ anticrossings are different. Although the same electron resonance is involved in both transitions, the voltages for the minimum splitting is different for the two cases. This is a very surprising result, since one would expect that the line splitting would be determined solely by the $e1$-$e2$ splitting, which is identical for the two transitions. Moreover, the minimum splittings have different magnitudes for the two transitions in the same sample. These are the key observations of this work. We show below that these effects are a consequence of the electron-hole Coulomb interaction, and that they can be explained quantitatively.

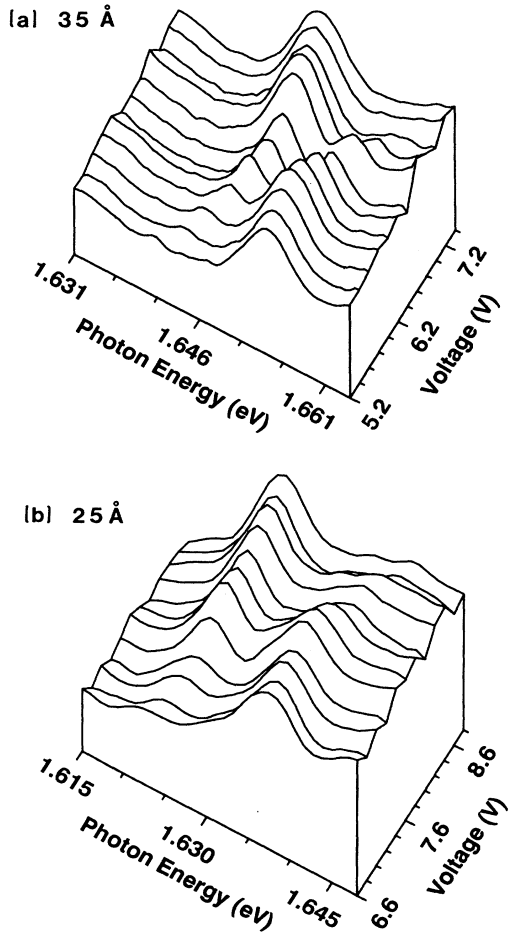

FIG. 7. 3D plot of the photocurrent spectra in the vicinity of the $H12$ transition as a function of reverse bias: (a) sample I at 30 K, (b) sample II at 50 K. Note that the photon-energy scale has been expanded compared to Fig. 5, and that the baseline has been offset for clarity. The absolute baseline position for (a) can be inferred from Fig. 4.

V. DISCUSSION

In the single-particle picture, we would observe transition energies as shown in Fig. 9 for the $H11$ and $H12$

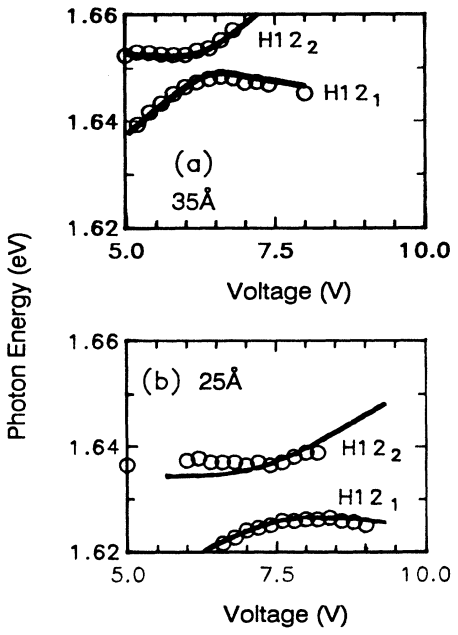

FIG. 8. $H12$ exciton energies versus applied bias: (a) sample I, (b) sample II. The solid lines are the results of the variational calculation using the same sample parameters as for the corresponding calculations for Fig. 6.

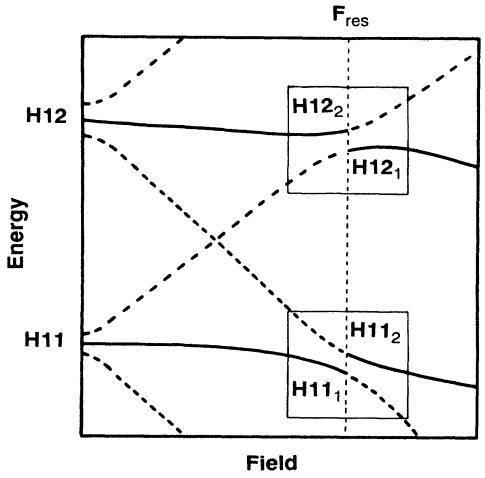

FIG. 9. Schematic field dependence of the $H11$ and $H12$ optical transition energies for the three-well system of Fig. 2 neglecting excitonic effects. Intrawell transitions are indicated by the solid lines, while interwell transitions are shown by the dashed lines.

transitions. The solid lines depict strong intrawell transitions, while the dashed lines indicate the weaker interwell transitions. The figure is drawn for the three wells of Fig. 2. At zero field the $e1$ levels of the three wells form a three-level miniband. On increasing the field, the three levels localize and fan out in a Stark ladder as shown in the figure. The same behavior is true for the $e2$ levels. The quantum-confined Stark effect adds a redshift to the transition energies at high fields.[36] This redshift is much smaller than the linear Stark shift of the interwell transitions arising from the potential drop between adjacent wells. The resonant field is simply the field for lining up the $e1$ and $e2$ levels of adjacent wells, which corresponds to the intersection point of the $H11$ and $H12$ intrawell and interwell transitions as shown in the figure. From the symmetry of the situation the "crossing point" must be the same for both transitions, as must be the splitting of the transitions at F_{res}. The subscripts attached to the transitions at the resonance refer to the number of wavefunction nodes.

Miniband and Stark-ladder behavior were only observed in the $e1$ levels of sample III in forward bias and also in reverse bias up to 1.5 V. At the higher values of reverse bias considered here, the $n=1$ heavy-hole absorption lines have a relatively small linewidth and show a strong quantum-confined Stark shift for all three samples. This behavior is characteristic of localized levels.[36] The $e2$ levels have a greater tendency to delocalization due to their lower confinement energy. The $n=2$ absorption lines were significantly broader than the $n=1$ lines (see, e.g., Fig. 4), but were still clearly resolvable for samples I and II, indicating substantial localization for the $e2$ levels at the field strengths of interest here. In sample III the $n=2$ transitions were weak at all field strengths, and only detectable as a shoulder around 1.65 eV. However, the fact that we observe a clear resonance in sample III indicates that the $e2$ level is at least partially localized at the field strengths studied here. A full treatment of the effect of the partially localized $e2$ miniband states in sample III at the resonant field is beyond the scope of this work. Our basic conclusions about the excitonic effects comes from considering the optical transitions in samples I and II, where we have experimental evidence that the $e2$ minibands are substantially broken up.

In a real optical experiment, exciton energies are measured rather than single particle splittings. In Fig. 10 we sketch the energy dependence of the exciton transitions associated with the $H11$ and $H12$ transitions close to the resonant field. The solid lines are a close-up of the single-particle resonance picture as shown in Fig. 9. The splitting is identical for both transitions in this picture. The dashed lines indicate what happens when the Coulomb interaction between the electron and hole is turned on. Let us concentrate first on the $H11$ transition. Below resonance, the $H11_1$ transition has intrawell character. The electron and hole are therefore predominantly in the same well, so that the Coulomb interaction will be strong, and thus the exciton will have a large binding energy (e.g., ~ 8 meV). By contrast, the $H11_2$ transition has interwell character with a reduced exciton binding because the electron and hole are localized in different quantum wells.[30] On sweeping through the resonance, the $H11_1$ transition switches over to an interwell transition, and vice versa for the $H11_2$ transition. Therefore, the exciton binding energy associated with each transition must also switch over at the resonance. In Fig. 10 we sketch this behavior. We have also sketched in the "crossing points," which are projections of the asymptot-

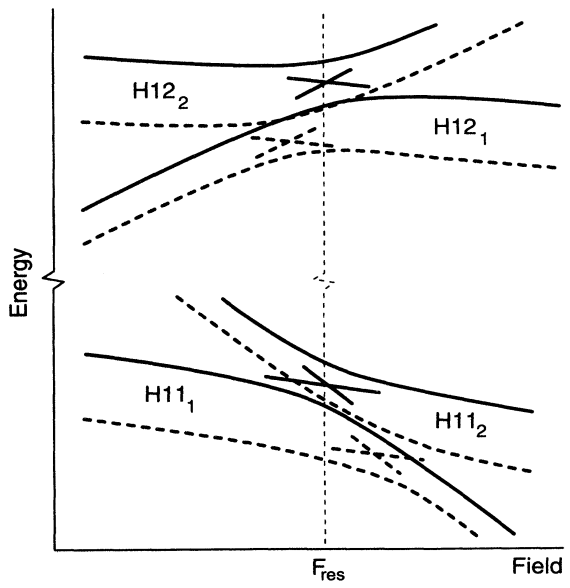

FIG. 10. Expanded version of Fig. 9 showing the detailed field-dependent optical transition energies close to resonance with (— — —) and without (——) the electron-hole Coulomb interaction.

ic behavior of the various transitions. These projected crossing points show that the point of minimum separation for the two $H11$ transitions is shifted to *higher* fields than $F_{\rm res}$, and that the minimum exciton line separation for the $H12$ transition now occurs *below* $F_{\rm res}$.

On comparing Figs. 9 and 10, one can see that the magnitude of the field shift ΔF for minimum line splitting is given approximately by

$$\frac{\Delta F}{F_{\rm res}} \approx \pm \frac{E_x^{\rm intra} - E_x^{\rm inter}}{E_2 - E_1} , \tag{1}$$

where $E_x^{\rm intra}$ and $E_u^{\rm inter}$ are the binding energies of intrawell and interwell excitons respectively, and E_2 and E_1 are the $e1$ and $e2$ sublevel energies at zero field. Formula (1) follows simply from the linearly projected crossing points in Fig. 10. The shift is positive for transitions terminating on the $e1$ level away from resonance, and negative for those which terminate on the $e2$ level. Inspection of Eq. (1) indicates that $\Delta F/F_{\rm res}$ will be largest in samples with small $(E_2 - E_1)$ (i.e., samples with large well widths) and/or samples with large $E_x^{\rm intra} - E_x^{\rm inter}$ (i.e., samples with larger separations of adjacent wells). Note that ΔF does *not* really depend on the strength of the coupling between the wells; we could replace a low barrier with a high barrier and make little difference to ΔF, although we would, of course, change the magnitude of the splitting and the oscillator strength of the interwell transitions.

We can compare the predictions of Eq. (1) with the experimental data. We find that the field for minimum level separation is larger for the $H11$ transition than for the $H12$ transition in both samples I and II, as predicted by our model. The shift in the voltage for minimum level separation between the two transitions is $\sim 10\%$ for both samples, and thus implies $\Delta F/F_{\rm res} \sim 5\%$. The ~ 100 meV experimentally determined energy separation between the $H11$ and $H12$ transitions therefore tells us that $(E_x^{\rm intra} - E_x^{\rm inter})$ is about 5 meV for our samples. Below we show how we can obtain a quantitative agreement between the experimental data and the exciton model from a variational calculation of the exciton binding energies and wave functions.

VI. VARIATIONAL EXCITON ENERGY CALCULATION

We calculated the field dependence of the exciton energies variationally using the following Hamiltonian:[36]

$$H = -\frac{\hbar^2}{2\mu_{xy}}\nabla_{xy}^2 - \frac{\hbar^2}{2m_e}\frac{\partial^2}{\partial z_e^2} - \frac{\hbar^2}{2m_h}\frac{\partial^2}{\partial z_h^2} - \frac{e^2}{4\pi\epsilon_0\epsilon_r r} \pm eFz_{e,h} + V_{e,h}(z_{e,h}) . \tag{2}$$

The subscripts e and h and the signs $-$ and $+$ refer to electrons and holes, respectively, for the field direction as in Figs. 1 and 2, z is the direction perpendicular to the layers, $r = [x^2 + y^2 + (z_e - z_h)^2]^{1/2}$, μ_{xy} is the x-y plane reduced effective mass, $m_{e,h}$ is the particle effective mass, and $V_{e,h}$ is the quantum-well potential. As a first approximation, we solve for the wave functions and single-particle energies without the Coulomb interaction and the x-y plane kinetic energy. In this approximation, the problem is separable into electron and hole Schrödinger equations according to

$$\left[-\frac{\hbar^2}{2m_{e,h}}\frac{\partial^2}{\partial z_{e,h}^2} \pm eFz_{e,h} + V_{e,h}(z_{e,h}) \right] \Psi_{e,h}(z_{e,h}) = E_{e,h}\Psi_{e,h}(z_{e,h}) . \tag{3}$$

This is just the standard equation for a particle in a quantum well with an applied perpendicular electric field, and gives rise to the quantum-confined Stark effect.[36] It can be solved by the tunneling resonance technique, for example.[36,37] In this way we can find the wave functions and Stark-shifted energies of the three levels of interest here: the two resonant $\{e1, e2\}$ electron sublevels with wave functions $\{\Psi_{e1}(z_e), \Psi_{e2}(z_e)\}$ and energies $\{E_{e1}, E_{e2}\}$, respectively (the subscripts 1 and 2 refer to the number of wave-function nodes), and the hh1 first heavy-hole sublevel with wave function $\Psi_{\rm hh1}(z_h)$ and energy $E_{\rm hh1}$. The wave functions shown in Fig. 3 are in fact the calculated normalized electron wave functions $\Psi_{e1}(z_e)$ and $\Psi_{e2}(z_e)$ for sample I.

The effect of the Coulomb interaction is to remix the nearly degenerate electron wave functions $\Psi_{e1}(z_e)$ and $\Psi_{e2}(z_e)$ in such a way as to minimize the energy. We performed a variational calculation to find the size of the mixing, using the following orthogonal trial wave functions for the exciton:

$$\begin{aligned} \Psi_+ &= [\alpha\Psi_{e1} + (1-\alpha^2)^{1/2}\Psi_{e2}]\Psi_{\rm hh1}\Phi_{1s}(\lambda) , \\ \Psi_- &= [-(1-\alpha^2)^{1/2}\Psi_{e1} + \alpha\Psi_{e2}]\Psi_{\rm hh1}\Phi_{1s}(\lambda) , \\ \Phi_{1s}(\lambda) &= \left[\frac{2}{\pi}\right]^{1/2}\frac{1}{\lambda}\exp\left[\frac{-(x^2+y^2)^{1/2}}{\lambda}\right] , \end{aligned} \tag{4}$$

where $(1 - |\alpha|)$ is the mixing amplitude and λ is the x-y plane $1s$ exciton diameter, both of which are to be found in the variational calculation. λ may be different for Ψ_+ and Ψ_-. Normalization requires that $|\alpha| \leq 1$. If there were no mixing, α would be either 0 or 1. The mixing is maximum when $\alpha = 1/\sqrt{2}$. Intuitively, we expect $|\alpha|$ to be close to unity except near $F_{\rm res}$.

In choosing these trial wave functions, we are assuming that the only states which undergo significant mixing are the two resonant electron levels. The reason behind this is that the exciton binding energy is ~ 10 meV, which is of the same order of magnitude as the unperturbed splitting of the two resonant electron levels. By contrast, the next closest electron level is ~ 100 meV away. We have neglected the mixing effects in the valence band. The approximation is well justified for the 35-Å sample, but less so for the 15-Å sample, where the splitting is ~ 20 meV and has to be compared to the hh1-hh2 separation of ~ 30 meV. A more sophisticated model would include the mixing of the heavy-hole sublevels, and possibly also the mixing between heavey-hole and light-hole sublevels. It would also need to include the effects of only partial localization of the $e2$ levels in sample III as discussed in Sec. V.

The variational calculation is greatly simplified by as-

suming that α must be real. This would be rigorously justified if the solutions of the Schrödinger equation were genuine eigenfunctions, in which case time-reversal symmetry permits the choice of real eigenfunctions without loss of generality. In our case, the calculated wave functions are not true stationary states because we are using a traveling-wave approach (the tunneling resonance method). However, since the wave-function amplitudes decay exponentially in the outer barriers, there is only a limited loss of generality in choosing real wave functions. Again, this approximation becomes more severe as the barrier thickness decreases.

On substituting Eq. (4) into the Schrödinger equation with the Hamiltonian of Eq. (2), we obtain the energies of the two excitons relative to the GaAs band gap as follows:

$$\begin{aligned} E_+ &= \alpha^2 E_{e1} + (1-\alpha^2)E_{e2} + E_{\mathrm{hh1}} + \frac{\hbar^2}{2\mu_{xy}\lambda^2} \\ &\quad - [\alpha^2 I_{11} + (1-\alpha^2)I_{22} + 2\alpha(1-\alpha^2)^{1/2} I_{12}] , \\ E_- &= (1-\alpha^2)E_{e1} + \alpha^2 E_{e2} + E_{\mathrm{hh1}} + \frac{\hbar^2}{2\mu_{xy}\lambda^2} \\ &\quad - [(1-\alpha^2)I_{11} + \alpha^2 I_{22} - 2\alpha(1-\alpha^2)^{1/2} I_{12}] , \end{aligned} \tag{5}$$

where the integrals I_{ij} are given by

$$\begin{aligned} I_{ij}(\lambda) &= \frac{2e^2}{4\pi\varepsilon_0\varepsilon_r\lambda} \int_{z_e} \int_{z_h} \Psi_{e_i}(z_e)\Psi_{e_j}(z_e) \\ &\quad \times |\Psi_{\mathrm{hh1}}(z_h)|^2 G(|z_e - z_h|) \\ &\quad \times dz_e\, dz_h , \\ G(\gamma) &= \frac{2}{\lambda} \int_{r=0}^{\infty} \frac{r \exp(-2r/\lambda)}{(\gamma^2 + r^2)^{1/2}} dr . \end{aligned} \tag{6}$$

The radial integral $G(\gamma)$ can be simplified into standard mathematical functions as explained in Ref. 36. The calculation proceeds by minimizing E_+ with respect to both α and λ. Once α has been found, we then minimize E_- with respect to λ at fixed α. In this way we obtain the mixing coefficient, and the Bohr radii of the two excitons considered. [The choice of wave functions in Eq. (4) assures orthogonality.] The exciton binding energies $E_x^{\pm}$ are readily obtained from

$$\begin{aligned} E_x^+ &= E_{e1} + E_{\mathrm{hh1}} - E_+ , \\ E_x^- &= E_{e2} + E_{\mathrm{hh1}} - E_- . \end{aligned} \tag{7}$$

Here we define the exciton binding energy to be the difference between the transition energies with and without the Coulomb interaction, consistent with the picture in Fig. 10.

In Fig. 11 we give an example of the calculated wave functions for sample I. The figure shows the unperturbed $\Psi_{e1}(z_e)$, $\Psi_{e2}(z_e)$, and $\Psi_{\mathrm{hh1}}(z_h)$ wave functions, together with the z_e part of the mixed wave functions $\Psi_{\pm}$. We see a very simple physical interpretation for the Coulomb mixing:[31] the localized holes have a tendency to attract the electrons in the lower state to their own well by increasing the electron wave-function amplitude in that particular well. As is often the case, the second level has to have the opposite "counterintuitive" behavior.

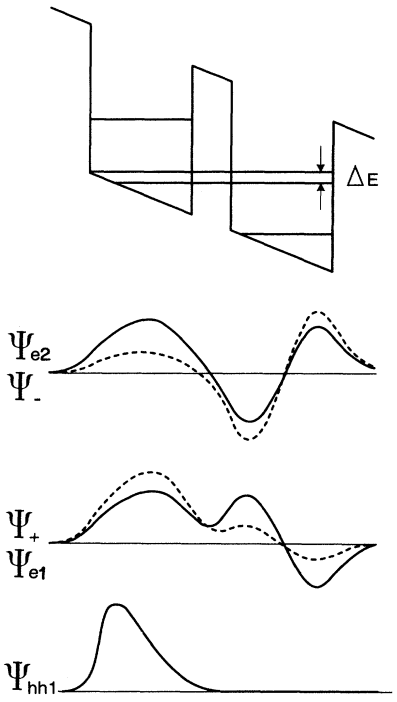

FIG. 11. Calculated electron and hole wave functions for sample I at 83 kV cm^{-1}, the field for minimum splitting of the "bare" electron levels. The electron wave functions are shown with (– – –) $\{\Psi_+, \Psi_-\}$ or without (——) $\{\Psi_{e1}, \Psi_{e2}\}$ the Coulomb interaction. Ψ_{hh1} is the wave function of the first heavy-hole subband.

The curves plotted over the data in Figs. 6 and 8 show the results of the variational calculation. The same parameters were used for a given sample to give the fits shown in the two figures. The best-fit values of L_w and L_b are given in Table II. In choosing these values, consideration was given not only to fitting the data given in Figs. 6 and 8, but also to fitting the other resolved transitions (see, e.g., Fig. 4). The x values were determined by fitting the optical-absorption edge of top p-type $Al_xGa_{1-x}As$ contact layer, and agree with the x-ray values given in Table I to within ±4%. We used $m_e = 0.0665$, $m_h = 0.34$, and $\mu_{x,y} = 0.0415$ for the effective masses of GaAs. For the $Al_xGa_{1-x}As$ we used $m_e = [0.067 + 0.093x]$ and $m_h = [0.34 + 0.42x]$. We used an averaged material-independent dielectric constant of 12.15. The band gaps used were 1.522 eV for GaAs and $[1.522 + 1.425x - 0.9x^2 + 1.1x^3]$ for the $Al_xGa_{1-x}As$. GaAs conduction-band nonparabolicity was included according to Eq. (64) of Ref. 38. The built-in voltage of the diode was used as a fitting parameter for the anticrossings, and the best values found for samples I–III were −1.65, −0.8, and −1.2 V, respectively. The values for samples I and III are in good agreement with low-temperature I-V measurements in the forward-bias direc-

TABLE II. Sample parameters used to generate the solid lines plotted over the data in Figs. 6 and 8 using the variational exciton energy calculation.

Sample	Well width (Å)	Barrier width (Å)	x	Total MQW thickness (μm)
I	89	35	0.33	0.99
II	97	25	0.27	1.13
III	92	15	0.28	0.97

tion. The value used for sample II is unrealistically low. This may indicate some field nonuniformity in that sample. The value of the band-offset ratio ΔE_c:ΔE_v used to generate the curves in Figs. 6 and 8 was 67:33. This value is based on determinations of ΔE_c:ΔE_v from optical measurements.[39–41] We discuss below the effect of changing ΔE_c:ΔE_v. On comparing Tables I and II we see that there are discrepancies of up to ~10% among the x-ray measurements, the design values, and the fit values.

Our calculations accurately reproduce the shift in field for the minimum splitting for the two transitions, and also give fairly close agreement with the absolute magnitude of the splittings over the entire voltage range studied. The difference in the field for minimum exciton splitting as opposed to electron level splitting is calculated to be about ±5% for all three samples, in good agreement with the experimental results for samples I and II. The fit is best for the 35-Å sample. With the thinner barrier samples, the approximations in our model become more significant, as discussed above. The calculated values of ΔE for the bare electron levels are 5.5, 11.4, and 22.2 meV for samples I–III, respectively.

As a further example of the results of the calculation, we show in Fig. 12 the binding energy of the $H11_1$ and $H11_2$ excitons as a function of voltage for sample I, together with the mixing parameter α. The binding energy of the intrawell exciton ranges from 8.2 meV at 5 V to 7.6 meV at 8 V, which should be compared to the interwell value of 3.7 and 3.6 meV at the same voltages. The switching behavior of the exciton binding energy on increasing the field through the resonance is evident. The calculated values of 4.0–4.5 meV for $(E_x^{\text{intra}}-E_x^{\text{inter}})$ agrees quite well with our rough estimate of 5 meV based on Eq. (1). Moreover, the absolute numbers for E_x^{intra} and E_x^{inter} compare favorably with other estimates in the literature.[30] The exciton radius $\lambda/2$ is about 70 Å for the intrawell exciton and 130 Å for the interwell exciton. The mixing parameter α is close to unity except at the resonant field, where it has its minimum value of 0.85. There is significantly less mixing for the $H12$ transition, where the minimum value of α is 0.98. The mixing also decreases with the decreasing barrier thickness, with the minimum values of α being 0.95 and 0.98 for the $H11$ excitons in the 25 and 15 Å samples, respectively. The decrease of mixing with decreasing barrier thickness is to be expected because the Coulomb interaction is relatively less important for samples with larger splittings.

In Fig. 13 we have plotted the experimental values for the minimum $H11$ exciton line splitting for the three

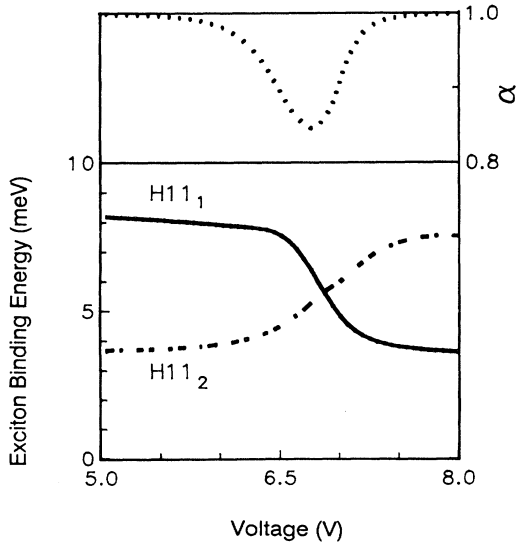

FIG. 12. Calculated $H11_1$ and $H11_2$ exciton binding energy versus applied reverse bias for sample I near the resonance point. The wave-function mixing parameter α for this transition is also shown.

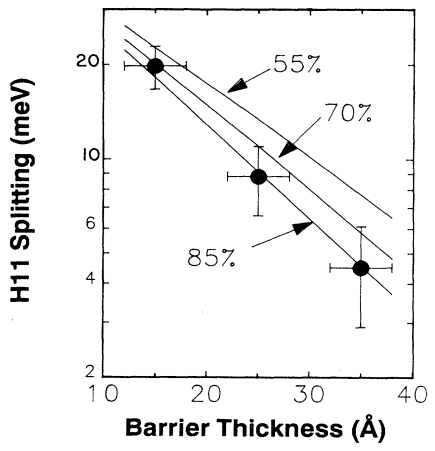

FIG. 13. Minimum $H11$ exciton line splitting against barrier thickness L_b. The near exponential dependence of the splitting of L_b is evident. The solid lines are theoretical curves generated for three different values of the fraction of the GaAs/$Al_xGa_{1-x}As$ band-gap discontinuity in the conduction band.

samples against L_b. We have used the fitted L_b values and indicate with an error bar the effect of a variation of ± 1 monolayer. The vertical error bars are calculated from our model to allow for a $\pm 10\%$ variation in the x value of the samples and a ± 5-Å variation in L_w. These vertical error bars are included to allow for the fact that the actual sample parameters differ from the design values. The solid lines are a calculation of the $H11$ exciton splitting for $L_w = 95$ Å and $x = 0.3$ for three different values of Q_e, the fraction of the band-gap discontinuity in the conduction band: $\Delta E_c/(\Delta E_c + \Delta E_v)$. We expect that the variation of the minimum electron sublevel splitting with barrier thickness should be exponential to first order.[1,14] The data points seem to follow the expected exponential dependence to within the experimental accuracy. The calculated exciton splittings depart very little from the basic exponential dependence of the sublevel splitting. In principle, accurate measurements of the line splitting against L_b should be able to determine $\Delta E_c/\Delta E_v$ to high precision because of the exponential sensitivity of the interwell coupling to the barrier height. The accuracy of this determination is limited by the reproducibility of the well width and x value from sample to sample. However, it does seem that values around 55:45, which have been previously used in some calculations, are too low.

VII. CONCLUSIONS

We conclude that great care needs to be taken when interpreting optical resonant-coupling measurements: the field dependence of the exciton line splitting corresponds neither conceptually nor quantitatively with the underlying single-particle state splitting. A full exciton model is required to explain the data completely. From our model we estimate that the fractional field shifts will be over 20% for samples with quantum-well widths around 200 Å. We have quantified these effects for an electron resonance in two specific optical transitions, but our conclusions have general applicability to all interband optical resonant tunneling experiments that measure exciton peaks. This applies equally well to both electron and hole resonances in superlattices or symmetric double-well structures, and it also applies to ground-to-ground resonant coupling in asymmetric double quantum wells. The effects will be most pronounced in samples where the difference in the binding energy of interwell and intrawell excitons is comparable to ΔE. These results are important for precise determinations of material parameters such as the band offset ratio, which in principle can be determined by measuring the variation of ΔE with L_b. Our conclusions will thus be important both for an improved understanding of optical resonant-coupling experiments, as well as in the design of coupled-quantum-well electroabsorptive devices.

ACKNOWLEDGMENTS

We would like to thank J. E. Henry and M. M. Becker for processing the samples. We are grateful to S. L. Chuang, D. S. Chemla, and G. W. t' Hooft for helpful comments and discussion.

*Present address: Clarendon Laboratory, Parks Road, Oxford OX1 3PU, United Kingdom.

†Present address: AT&T Bell Laboratories, Solid State Technology Center, Breinigsville, PA 18031.

[1] E. O. Kane, in *Tunneling Phenomena in Solids,* edited by E. Burnstein and S. Lundqvist (Plenum, New York, 1969), p. 1.

[2] R. F. Kararinov and R. A. Suris, Fiz. Tekh. Poluprovodn. **5**, 797 (1971) [Sov. Phys.—Semicond. **5**, 707 (1971)].

[3] T. Furuta, K. Hirakawa, J. Yoshino, and H. Sakaki, Jpn. J. Appl. Phys. **25**, L151 (1986).

[4] F. Capasso, K. Mohammed, and A. Y. Cho, IEEE J. Quantum Electron. **QE-22**, 1853 (1986).

[5] H. Q. Le, J. J. Zayhowski, and W. D. Goodhue, Appl. Phys. Lett. **50**, 1518 (1987).

[6] S. L. Chuang and B. Do, J. Appl. Phys. **62**, 1290 (1987).

[7] Y. J. Chen, E. S. Koteles, B. S. Elman, and C. A. Armiento, Phys. Rev. B **36**, 4562 (1987).

[8] K. K. Choi, B. F. Levine, C. G. Bethea, J. Walker, and R. J. Malik, Phys. Rev. Lett. **59**, 2459 (1987).

[9] S. R. Andrews, C. M. Murray, R. A. Davies, and T. M. Kerr, Phys. Rev. B **37**, 8198 (1988).

[10] M.-H. Meynadier, R. E. Nahory, J. M. Worlock, M. C. Tamargo, J. L. de Miguel, and M. D. Sturge, Phys. Rev. Lett. **60**, 1338 (1988).

[11] R. Sauer, K. Thonke, and W. T. Tsang, Phys. Rev. Lett. **61**, 609 (1988).

[12] J. E. Golub, P. F. Liao, D. J. Eilenberger, J. P. Harbison, L. T. Florez, and Y. Prior, Appl. Phys. Lett. **53**, 2584 (1988).

[13] H. Schneider, K. von Klitzing, and K. Ploog, Superlatt. Microstruct. **5**, 383 (1989).

[14] S. Tarucha and K. Ploog, Phys. Rev. B **39**, 5353 (1989).

[15] Y. Tokuda, K. Kanamoto, N. Tsukada, and T. Nakayama, Appl. Phys. Lett. **54**, 1232 (1989).

[16] H. Schneider, W. W. Rühle, K. v. Klitzing, and K. Ploog, Appl. Phys. Lett. **54**, 2656 (1989).

[17] T. B. Norris, V. Vodjdani, B. Vinter, C. Weisbuch, and G. A. Mourou, Phys. Rev. B **40**, 1392 (1989).

[18] G. Livescu, A. M. Fox, D. A. B. Miller, T. Sizer, W. H. Knox, A. C. Gossard, and J. H. English, Phys. Rev. Lett. **63**, 438 (1989).

[19] D. Y. Oberli, J. Shah, T. C. Damen, C. W. Tu, Y. T. Chang, D. A. B. Miller, J. E. Henry, R. F. Kopf, N. Sauer, and A. E. DiGiovanni, Phys. Rev. B **40**, 3028 (1989).

[20] C. C. Phillips, R. Eccleston, and S. R. Andrews, Phys. Rev. B **40**, 9760 (1989).

[21] H. Sakaki, T. Matsusue, and M. Tsuchiya, IEEE J. Quantum Electron. **QE-25**, 2498 (1989).

[22] G. Bastard, C. Delalande, R. Ferreira, and H. W. Liu, J. Lumin. **44**, 247 (1989).

[23] Y. Tokuda, K. Kanamoto, and N. Tsukada, Appl. Phys. Lett. **56**, 166 (1990).

[24] H. T. Grahn, H. Schneider, W. W. Rühle, K. v. Klitzing, and K. Ploog, Phys. Rev. Lett. **64**, 2426 (1990).

[25] K. Leo, J. Shah, E. O. Göbel, T. C. Damen, K Köhler, and

Peter Ganser, Appl. Phys. Lett. **56**, 2031 (1990).
[26]Q. Xu, Z. Y. Xu, J. Z. Xu, B. Z. Zheng, and H. Xia, Solid State Commun. **73**, 813 (1990).
[27]H. Schneider, H. T. Grahn, K. v. Klitzing, and K. Ploog, Phys. Rev. B **40**, 10 040 (1989).
[28]K. Leo, J. Shah, J. P. Gordon, T. C. Damen, D. A. B. Miller, C. W. Tu, and J. E. Cunningham, Phys. Rev. B **42**, 7065 (1990).
[29]J. Lee, M. O. Vassel, E. S. Koteles, and B. Elman, Phys. Rev. B **39**, 10 133 (1989).
[30]J. E. Golub, P. F. Liao, D. J. Eilenberger, J. B. Harbison, and L. T. Florez, Solid State Commun. **72**, 735 (1989).
[31]I. Galbraith and G. Duggan, Phys. Rev. B **40**, 5515 (1989).
[32]T. Kamizato and M. Matsuura, Phys. Rev. B **40**, 8378 (1989).
[33]A. M. Fox, D. A. B. Miller, G. Livescu, J. E. Cunningham, J. E. Henry, and W. Y. Jan, Phys. Rev. B **42**, 1841 (1990).
[34]T. Fukuzawa, E. E. Mendez, and J. M. Hong, Phys. Rev. Lett. **64**, 3066 (1990).
[35]E. E. Mendez, F. Agulló-Rueda, and J. M. Hong, Phys. Rev. Lett. **60**, 2426 (1988).
[36]D. A. B. Miller, D. S. Chemla, T. C. Damen, A. C. Gossard, W. Wiegmann, T. H. Wood, and C. A. Burrus, Phys. Rev. B **32**, 1043 (1985).
[37]D. A. B. Miller, J. S. Weiner, and D. S. Chemla, IEEE J. Quantum Electron. **QE-22**, 1816 (1986); for a recent review of quantum-well electroabsorption, see S. Schmitt-Rink, D. S. Chemla, and D. A. B. Miller, Adv. Phys. **38**, 89 (1989).
[38]J. S. Blakemore, J. Appl. Phys. **53**, R123 (1982).
[39]J. Menendez, A. Pinczuk, A. C. Gossard, J. H. English, D. J. Werder, and M. G. Lamont, J. Vac. Sci. Technol. B **4**, 1041 (1986).
[40]D. J. Wolford, T. F. Kuech, J. A. Bradley, M. A. Gell, D. Ninno, and M. Jaros, J. Vac. Sci. Technol. B **4**, 1043 (1986).
[41]K. J. Moore, P. Dawson, and C. T. Foxon, Phys. Rev. B **38**, 3368 (1988).